Clim. Past Discuss., https://doi.org/10.5194/cp-2017-146
Manuscript under review for journal Clim. Past
Discussion started: 24 November 2017

Climate of the Past
Discussions

A Stalagmite Test of North Atlantic SST and Iberian Hydroclimate Linkages over the Last Two Glacial Cycles

Rhawn F. Denniston[a*], Amanda N. Houts[a1], Yemane Asmerom[b], Alan D. Wanamaker, Jr.[c], Jonathon A. Haws[d], Victor J. Polyak[b], Diana L. Thatcher[c], Sestsen Altan-Ochir[a], Alyssa C. Borowske[a2], Sebastian F.M. Breitenbach[e], Caroline C. Ummenhofer[f], Frederico T. Regala[g], Michael M. Benedetti[h], Nuno Bicho[i]

[a] Department of Geology, Cornell College, Mount Vernon, Iowa 52314 USA
[b] Department of Earth and Planetary Sciences, University of New Mexico, Albuquerque, New Mexico 87131 USA
[c] Department of Geological and Atmospheric Sciences, Iowa State University, Ames, Iowa 50011 USA
[d] Department of Anthropology, Louisville University, Louisville, Kentucky 40208 USA
[e] Institute for Geology, Mineralogy, and Geophysics, Ruhr-University Bochum 44801 Germany
[f] Department of Physical Oceanography, Woods Hole Oceanographic Institution, Woods Hole, Massachusetts 02543 USA
[g] Associação de Estudos Subterrâneos e Defesa do Ambiente, Torres Vedras, Portugal
[h] Department of Geography and Geology, University of North Carolina Wilmington, Wilmington, North Carolina 28403 USA
[i] Center for Archaeology and Evolution of Human Behaviour, Universidade do Algarve, Faro, Portugal

[*] corresponding author

[1] current address: Department of Earth Sciences, University of New Hampshire, Durham, New Hampshire 03824 USA
[2] current address: Department of Ecology and Evolutionary Biology, University of Connecticut, Storrs, Connecticut 06269 USA

Keywords
Iberia, hydroclimate, stalagmite, carbon isotope, $\delta^{234}U$, pollen, sea surface temperature

Abstract

Close coupling of Iberian hydroclimate and North Atlantic sea surface temperature (SST) during recent glacial periods has been identified through the analysis of marine sediment and pollen grains co-deposited on the Portuguese continental margin. These reconstructions have lacked a directly-dated, site-specific record of continental Iberian climate spanning multiple glacial cycles as a point of comparison. Here we present a high-resolution, multi-proxy ($\delta^{13}C$, $\delta^{234}U$, and growth dynamics) stalagmite record of hydroclimate from two caves in western Portugal across the majority of the last two glacial cycles (~230 ka). At orbital and millennial scales, stalagmite-based proxies of hydroclimate covaried with sea surface temperature (SST), with positive carbon isotope excursions and/or growth hiatuses indicating reduced effective moisture coincident with suppressed SST during major ice-rafted debris events and Greenland stadials, in agreement with changes in palynological reconstructions of continental climate. The Portuguese stalagmite record also reveal intervals during which the magnitudes of hydroclimate changes appear to have been somewhat decoupled from SST.

1. Introduction

The Portuguese continental margin is an important location for understanding oscillations in paleoceanographic conditions over orbital and millennial-scales (e.g., Voelker and de Abreu, 2011). Here, marine sediments record basin-wide oceanographic signals while co-deposited pollen grains track coeval vegetation changes occurring across Iberia. Integrated analysis of these proxies has revealed a close coupling of North Atlantic SST, regional climate, and Iberian ecosystems during the last three glacial cycles, including changes in vegetation dynamics (Sánchez Goñi et al., 2002; Tzedakis et al., 2004; Roucoux et al., 2006; Martrat et al., 2007;

Naugthon et al. 2007; Sánchez Goñi et al., 2008), atmospheric circulation (Sánchez Goñi et al., 2013), and fire frequency (Daniau et al., 2007). One commonly applied palynological metric is the abundance of temperate tree pollen, which rises during warm and wet conditions associated both with interglacials and Greenland interstadials, concomitant with shifts in Iberian margin SST (Sánchez Goñi et al., 2002; Tzedakis et al., 2004; Combourieu-Nebout et al., 2009; Fletcher et al., 2010; Chabaud et al., 2014). However, the nature of such land-sea connections is partially obscured by the size of catchments from which the pollen are derived, with some reaching into central Iberia and spanning a range of environmental settings subject to varying climate influences (Martin-Vide and Lopez-Bustins, 2006; Naughton et al., 2007) (Fig. 1).

Testing the links between terrestrial and marine systems requires continental climate proxies that provide precisely-dated and high resolution rainfall-sensitive time series spanning tens of millennia, but such records remain rare in Iberia, particularly near the west Iberian margin (Fletcher et al., 2010; Moreno et al., 2012; Stoll et al., 2013). Here we present a stalagmite record of three proxies for hydroclimate – growth dynamics, $^{13}C/^{12}C$ ratios ($\delta^{13}C$), and $^{234}U/^{238}U$ ratios ($\delta^{234}U$) – spanning the majority of the last and penultimate glacial cycles (~230 ka) at two cave sites in western Portugal. This time series offers a rare, site-specific continental record capable of examining the coherence of SST controls on Iberian climate and ecosystem dynamics across glacial and interglacial periods. Few speleothem records exist in western Iberia, and this new speleothem record provides a continental proxy of hydroclimate linked to regional oceanographic conditions.

2. Samples and Regional Setting

We report the analysis of six stalagmites (BG41, BG66, BG67, BG68, BG611, BG6LR) from Buraca Gloriosa (BG; 39º32'N, 08º47'W; 420 m a.s.l.) and one stalagmite (GCL6) from Gruta do Casal da Lebre (GCL; 39˚18'N, 9˚16'W; 130 m a.s.l.), two caves in western Portugal (Fig. 1). Environmental conditions in BG and GCL are well suited for speleothem paleoclimate reconstruction. Each cave contains only a single, small (<1 m^2) entrance that restricts airflow and maintains stable temperatures (~1˚C change between summer and winter seasons) and high relative humidity (~100% perennially) throughout the year, despite the fact that drip rates are highly variable, corresponding to both seasonal climatology and individual rainfall events (Fig. 2).

BG and GCL are located in western Portugal, an area within the Meso-Mediterranean bioclimatic zone that dominates much of Iberia (Fig. 1). This region is characterized by strong seasonality, with warm, dry summers and cool, wet winters (Fig. 3) associated with the winter westerlies (Blanco Castro et al., 1997). In contrast, the Atlantic zone, north of the Douro River, is cooler, wetter, and less strongly seasonal. In the Pleistocene, the transition between these zones likely shifted southward with Mediterranean-type vegetation restricted to refugia (Rey Benayas and Scheiner, 2002). Pollen is transported to the west Iberian margin largely via major stream systems including (from north to south) the Douro, Tagus, and Sado rivers, with large watersheds (79,000, 81,000, and 7,650 km^2, respectively). The Tagus and Sado are primarily responsible for pollen deposited southwest of Portugal, while the Douro plays an important role in delivering pollen to the more northwesterly sites (Fig. 1). Prevailing wind patterns likely prevent substantial transport of pollen from Iberia to the western Portuguese margin (Naughton et al., 2007).

Today, the hydroclimate of western Iberia is tightly coupled with the winter North Atlantic Oscillation (NAO) (Fig. 4), an atmospheric dipole that strongly influences precipitation across much of western Europe and that more broadly reflects the strength and positioning of the Azores high-pressure system, which steers storm tracks contained within the westerlies into or north of Iberia (e.g., Trigo et al, 2002; Paredes et al., 2006; Trouet et al., 2009; Cortesi et al., 2014). The NAO is typically measured as the NAO index, which is calculated using atmospheric pressure differences between Iceland and Lisbon (or the Azores) (Barnston and Livezey, 1987). The nature of the influence of the NAO varies across Iberia, but it is strongly correlated to rainfall in western Portugal (Fig. 4). A positive NAO index is associated with a larger pressure gradient and elevated Iberian aridity. Iberian precipitation has also been linked closely to SST in regions ranging from the western North Atlantic to the Iberian margin (Lorenzo et al., 2010) where ocean circulation is dominated by the southward-flowing Portugal Current and the near-coastal and north-flowing Iberian Poleward Current, two systems that transport pollen from river mouths along the continental shelf (Fig. 1).

3. Materials and Methods

Stalagmite chronologies were constructed with a total of 76 ^{230}Th dates obtained at the University of New Mexico (Table 1) using the methods of Asmerom et al. (2010). For GCL samples, corrections for unsupported ^{230}Th were made with the global ^{230}Th/^{232}Th crustal silicate value of 4.4 ppm (±50%), and for BG, corrections were made using a ratio of 13.5 ppm (±50%), a value determined from isotopic analysis of cave drip water. Powders ranging from 50-150 mg transferred into 30 ml Teflon beakers, weighed, dissolved in 15N nitric acid, and then spiked with a mixed ^{229}Th-^{233}U-^{236}U tracer and processed using column chemistry methods. U and Th

Clim. Past Discuss., https://doi.org/10.5194/cp-2017-146
Manuscript under review for journal Clim. Past
Discussion started: 24 November 2017

fractions were dissolved in 5 ml of 3% nitric acid and transferred to analysis tubes for measurement on the Thermo NEPTUNE MC-ICP-MS. U and Th isotopic ratios were aspirated into the MC-ICP-MS using a Cetac Aridus II low flow desolvating nebulizer and run as static routines. All isotopes of interest were measured in Faraday cups, except for ^{234}U and ^{230}Th, which were measured in the secondary electron multiplier (SEM). Gains between the SEM and the Faraday cups were determined using standard solutions of NBL-112 for U and an in-house ^{230}Th-^{229}Th standard for Th which was measured after every fifth sample; chemistry blanks reveal U and Th blanks below 20 pg. Ages are reported using two standard deviation errors and are reported relative to the year AD 1950. Age models were developed via multiple polynomial interpolations between dated intervals using the COPRA age modeling software (Breitenbach et al., 2012), except for BG68, the chronology of which was determined by linear interpolation between the two U-series dates that represent a short interval of stalagmite growth (Fig. 5).

A total of 1,490 stable isotope analyses were performed on calcite samples milled from the central axis of each stalagmite. After milling, powders were weighed (~200 μg) and transferred to reaction vessels that were flushed with ultra-pure helium. Next, samples were digested using H_3PO_4 and equilibrated overnight (~15 hours) at 34°C before being analyzed. Isotopic ratios were measured using a GasBench II with a CombiPal autosampler coupled to a ThermoFinnigan Delta Plus XL mass spectrometer at Iowa State University. A combination of internal and external standards were run after every fifth sample, as well as before and after each batch, in order to ensure reproducibility. Oxygen and carbon isotope values are presented in parts per mil (‰) relative to the Vienna Pee Dee Belemnite carbonate standard (VPDB). Precision is better than 0.1‰ for both δ^{13}C and δ^{18}O.

The nature of the calcite comprising the BG samples alternates between a faster-growing, white, fibrous mineralogy and slower-growing, dense, clear fabric. In some areas of three samples - BG6LR, BG67, and BG68 - sharp changes between the two forms within the same growth horizons mark intervals of recrystallization. BG6LR, which grew discontinuously over much of the last glacial cycle, suffered from alteration of early Holocene (~10-7 ka) material, which was therefore excluded from this analysis. BG67 is characterized primarily by fibrous calcite that has been recrystallized to clear, dense calcite in a narrow band ascending through its core. U/Th dates from the fibrous calcite on the margins of the growth surface reveal open system behavior and thus this portion of BG67 was also excluded. BG68 is composed entirely of clear calcite but contains intervals of porosity, possibly originating from secondary alteration. We restricted our sampling to the central area of the stalagmite where calcite is clear, dense, and contains well-defined lamina. Growth position changed at numerous times in several of these stalagmites (Figure S1), and our sampling strategy accounted for these changes so as to consistently collect samples for stable isotopic analysis from the top surface (cap) of each stalagmite.

Environmental conditions were measured at both cave sites over a two-year period, with data measured in three-hour intervals near the areas where the stalagmites were deposited. Temperature and relative humidity were obtained using HOBO U23 automated sensors while barometric pressure was recorded with a HOBO U20L. Drip rates were monitored with a Stalagmate acoustic drip counter (Collister and Mattey, 2008) (Fig. 2)

4. Results

^{234}U-^{230}Th dating of BG and GCL stalagmites reveals growth across approximately three quarters of the last 230 ka, with periods of deposition interrupted by numerous hiatuses of varying length. The longest gaps in this record span 210-198, 160-149, 106-87, 71-61, and 44-36 ka, and integrating these records yields a quasi-continuous time series from MIS 9 to present. Additional periods of deposition are present but were excluded from this analysis due to signs of secondary alteration that raise questions about the accuracy of associated U/Th dates (Fig. S1). The large number of hiatuses and also changes in growth direction complicate construction of a reliable chronology in some intervals. However, multiple stalagmites span the same growth periods, allowing for replication tests of coeval material. Replication between stalagmites of similar age is arguably the single most reliable method for evaluating the impacts of climate vs disequilibrium influences on isotopic ratios (Dorale and Liu, 2009). The similar carbon isotopic trends and values across many of the areas of overlap argue for a consistent climate signal as the primary driver of isotopic variability (Fig. S2).

Hydroclimate is reconstructed here using a combination of stalagmite growth intervals and isotopic compositions. In some instances, deposition of multiple stalagmites was punctuated by hiatuses of similar time spans, a relationship that suggests links to changes in hydroclimate rather than random drip site-specific variability. Complementing growth intervals are stalagmite carbon isotopic ratios, which are impacted by a wide array of factors including vegetation type (plants utilizing the C_3 vs C_4 photosynthetic pathway) (Dorale et al., 1992) and density over the cave (Hellstrom and McCulloch, 2000), soil respiration rates (Genty et al., 2003), out-gassing of dissolved CO_2 from infiltrated water in voids in the epikarst under dry conditions (prior calcite precipitation; Baker et al., 1997), rate of CO_2-degassing from water entering the cave (Breitenbach et al., 2015), and isotopic disequilibrium during carbonate crystallization (e.g., Fairchild et al., 2006). Terrestrial deposits preserving pollen spectra spanning substantial portions of the last glacial cycle are not well known from western Iberia (Gómez-Orellana et al., 2008; Fletcher et al., 2010; Moreno et al., 2012), and thus pollen in ocean sediments represents a particularly important continental climate record. Pollen obtained from the Iberian margin reveal small percentages of *Poaceae*, the family including the majority of C_4 plants, and therefore a persistent and overwhelming majority of C_3 vegetation throughout the last glacial cycle including between Greenland stadials (GS) and interstadials (GI) and across Heinrich stadials (HS) (d'Errico and Sánchez Goñi, 2003; Tzedakis et al., 2004; Desprat et al., 2006; Sánchez Goñi et al., 2008; Sánchez Goñi et al., 2013; Margari et al., 2014) (Fig. 6). Thus, increases in carbon isotopic ratios are interpreted here as primarily reflecting a combination of desaturation of voids above the cave and decreased organic CO_2 production within the soil zone, both of which are consistent with a vegetative response to cooler, more arid climates (Baker et al., 1997; Genty et al., 2003).

Supporting this interpretation is the observed covariation of $\delta^{234}U$ and $\delta^{13}C$ values at both millennial and orbital scales (Fig. 6). During infiltration, ^{234}U is selectively mobilized relative to ^{238}U from the crystal lattices in carbonate bedrock owing to its displacement by alpha recoil during decay from ^{238}U (Chabaux et al., 2003; Oster et al., 2012). Decreases in effective precipitation and/or bedrock dissolution rate, both of which are associated with increased aridity, have been tied to elevated speleothem $\delta^{234}U$ values (Hellstrom and McCulloch, 2000; Plagnes et al., 2002; Polyak et al., 2012), and are interpreted similarly here. Thus, as precipitation/effective moisture decreased, stalagmite $\delta^{13}C$ and $\delta^{234}U$ values increased. As differences in $\delta^{234}U$ values between stalagmites may arise from distinct infiltration pathways, we restrict this part of the

Clim. Past Discuss., https://doi.org/10.5194/cp-2017-146
Manuscript under review for journal Clim. Past
Discussion started: 24 November 2017

analysis solely to stalagmite BG6LR, which represents the longest individual stalagmite record of this time series.

Oxygen isotope variability largely tracks that exhibited by carbon isotopes (Fig. S2). However, interpreting changes in oxygen isotope composition in this system during intervals of profound climatic change such as marked the last glacial period is complicated by the multiple factors that influenced $\delta^{18}O$ values of precipitation at these sites, including shifts in air temperature and rainfall amount (Fig. 3), as well as the potential for changes in atmospheric moisture sources on synoptic and seasonal scales (Moreno et al., 2014; Gimeno et al., 2012). Oxygen isotopic ratios in stalagmites may also be influenced by kinetic effects (Mickler et al., 2004) and evaporation above the cave (Denniston et al., 1999). For these reasons, the carbon isotopic record of BG/GCL represents the primary focus of this analysis. The reproducibility of carbon isotope ratios between coeval BG stalagmites argues that their $\delta^{13}C$ values may be viewed as an integrated time series not substantially impacted by inter-sample isotopic offsets (Fig. 6). However, incorporating the single GCL stalagmite into the BG record is complicated by site-specific cave hydrological effects, local controls on vegetation and soil formation, and different bedrock $\delta^{13}C$ values between the two caves that affect the values, although not the trends, of stalagmite carbon isotopic ratios (Fairchild et al., 2006). As a result, $\delta^{13}C$ values of this stalagmite are plotted separately in some figures to better track reconstructed Iberian SST.

The consistency and coherence among carbon (and oxygen) isotope values of coeval stalagmites support the interpretation that $\delta^{13}C$ values robustly record a paleoenvironmental signal (Dorale and Liu, 2009; Ridley et al., 2015). Some offsets exist, however, the most notable of which is the shift toward higher $\delta^{13}C$ values at the MIS 5e/6 transition (~130 ka) in stalagmite BG611 that contrasts with the sharp decrease in carbon isotopic ratios in BG67 (Fig. 6).

Assessing equilibrium crystallization in modern calcite/drip water pairs at BG is complicated by the substantial variability in integrated, months-long dripwater samples (average $\delta^{18}O$ value of -3.4 ± 1.1‰) and any seasonal biases in calcite crystallization that at present remain poorly constrained. However, combining these data with the average cave temperature (14.2±0.5°C) yields modeled calcite values of -3.3±1.6‰ (Kim and O'Neil, 1997), a value that lies in broad agreement with the oxygen isotopic composition of recently deposited BG stalagmite calcite (-3.1‰).

5. Environmental Conditions at BG/GCL and Links to the Iberian Margin

Over the last several glacial cycles, oceanographic conditions along the western Iberian margin varied at millennial and orbital time scales in close correlation with the North Atlantic (Roucoux et al., 2005; Daniau et al., 2007; Sánchez Goñi et al., 2008; Darfeuil et al., 2015). Abrupt changes in SST reflect a balance between southward expansion of cold, subpolar waters and northward migration of subtropical water masses (de Abreu et al., 2003). During the particularly cold conditions characterizing HS and GS, Iberian margin SST decreased by as much as 9˚C (to as much as 13˚C below present values; de Abreu et al., 2003), with these changes helping to position the arctic or subarctic front at ~39˚N, the same latitude as BG and GCL, thereby reducing atmospheric moisture to Iberia (Eynaud et al., 2009; Voelker and de Abreu, 2011). These oceanographic/atmospheric interactions would have influenced speleothem growth and carbon isotopic values at BG and GCL through impacts on effective moisture, vegetation density, and prior calcite precipitation. Indeed, the composite BG/GCL record documents a strong coherence, at both orbital and millennial scales, between Portuguese hydroclimate, vegetation, and Iberian margin SST during the last two glacial cycles (Fig. 6; Fig.

7). Stalagmite $\delta^{13}C$ and $\delta^{234}U$ values covary with baseline changes in SST, and are sensitive to gradual SST shifts. Millennial-scale changes in stalagmite carbon isotope ratios are more pronounced, with increased $\delta^{13}C$ and $\delta^{234}U$ values marking deterioration of Iberian climate associated with onset of cold, dry conditions during HS (Eynaud et al., 2009; Naughton et al., 2009; Voelker and de Abreu, 2011) (Fig. 7).

Growth hiatuses characterize HS3, HS4, and HS11, suggesting complete cessation of stalagmite deposition. Vegetation patterns during maximal IRD deposition on the Iberian margin reveal not only dramatically reduced forest cover but also a pronounced expansion of semi-desert plants, reflecting a further increase in aridity (e.g. Sánchez Goñi et al., 2000; Roucoux et al., 2005; Naughton et al., 2009). In particular, the long hiatus between HS7 and HS6 coincides with a period characterized by very low arboreal pollen abundances and expansion of semi-desert plants (Roucoux et al., 2005) and overlaps with the some of the coldest SST of the last 70 ka as reconstructed using $U^{k}_{37}{}'$ at core MD95-2042, a core from off the southwestern Iberian coast (Darfeuil et al., 2016).

Whether an absence of speleothem deposition is a result of pronounced reductions in precipitation, an extension of below freezing temperatures that limited infiltration (Vaks et al., 2013; Fankhauser et al., 2016), or variations in infiltration pathway/drip position is unclear. Pollen transfer functions from MD95-2042 (Fig. 1) suggest winter temperatures dropped below 0°C during HS and annual precipitation was reduced by up to 50% (from 800 mm to 500-400 mm during HS3, HS4, and HS5) (Sánchez Goñi et al., 2002). Applying this temperature reconstruction to western Portugal is complicated, however, by the broad area across which these pollen were sourced. Permafrost reconstructions (Vandenberghe et al., 2014) argue against the hypothesis that continuous sub-zero temperatures inhibited infiltration and stalagmite growth.

We thus suggest that the hiatuses observed at BG and GCL were driven largely by reductions in precipitation. This inference is supported by the discontinuous nature of stalagmite deposition during MIS 7 (221-193 ka). At this time, growth occurred in three intervals - MIS 7a, 7c, and 7e - punctuated by hiatuses during periods of ocean cooling (Fig. 2) and that also coincide with reductions in aquatic pollen and expansion of semi-desert plants (Desprat et al., 2006; Roucoux et al., 2006; Martrat et al., 2007; Voelker and de Abreu, 2011). During MIS 6, an absence in BG stalagmite deposition from ~160-149 ka (Fig. 6) occurs at the same time as massive seasonal discharges from the Fleuve Manche river and coldest continental climates and SST (157-154 ka) as determined from pollen and foraminifera from core MD01-2444 (Margari et al., 2014; Fig. 1). Stalagmites from Villars Cave, southwestern France, also contain hiatuses at 67-61, coincident with HS6, and 79-76 ka (Genty et al., 2003), similar in timing to hiatuses in the BG record at 71-60 and 80-78 ka (Fig. 1; Fig. 2). Additionally, a suite of stalagmites from multiple caves in northwestern Spain reveals punctuated growth, with periods of stalagmite deposition and/or elevated growth rates occurring during high Northern Hemisphere summer insolation or during GI (Stoll et al., 2013) (Fig. 1). Together, these data sets demonstrate a lack of stalagmite growth at times similar to those punctuating the BG/GCL record, suggesting SST controls on regional hydroclimate (Fig. 6).

Stalagmite carbon isotopic variations also track SST changes. Prominent positive carbon isotopic excursions define the Younger Dryas (YD), HS2, HS5, HS6, and HS8, consistent with diminished concentrations of arboreal pollen in cores from the Iberian margin, and document particularly cold and dry conditions (Sánchez Goñi et al., 2000; Roucoux et al., 2005; Sánchez Goñi et al., 2008) (Fig. 7). Reduced stalagmite $\delta^{13}C$ values document enhanced effective moisture from 170-160 and 145-135 ka, tracking peaks in temperate tree pollen and alkenone-based SST. Similarly, the sharp isotope shift marking the YD in the Portuguese stalagmite is consistent with the highest resolution SST record from the Iberian margin that reveals pronounced cooling during this time (Rodrigues et al., 2010).

Hydroclimatic shifts associated with GS and GI are also clearly expressed in some portions of the BG carbon isotope record, with the magnitude of carbon isotopic variability associated with GS/GI transitions ranging from 3-6‰ (Fig. 8). Pollen from the Iberian margin has been demonstrated to track GS/GI variations, with prominent changes occurring in relative abundances of Mediterranean and Atlantic forest and steppe vegetation (e.g., Sánchez Goñi et al., 2008). Other European stalagmite records have identified GI/GS events from the last glacial period (Genty et al., 2003; Spötl et al., 2006; Boch et al., 2011; Moseley et al., 2014), but the level of resolution recorded in the BG/GCL time series has not been clearly identified previously in western Iberia. Interesting, many GS/GI oscillations are not readily apparent during MIS 3, perhaps due to either insufficiently fine temporal resolution or a subdued hydroclimatic response. A carbon isotope time series (albeit with low temporal resolution) of a flowstone from southeast Spain does not present clear evidence of either GI or most HS during the last glacial cycle, although it does contain a clear expression of HS11 (Hodge et al., 2008) (Fig. 1). And while some Iberian lakes and peat bogs document environmental changes concurrent with HE, no single record, including one of the longest - the 50 ka time series from the Fuentillejo maar, south-central Spain - contains a consistent signal for all HS (Vegas et al., 2010; Moreno et al., 2012) (Fig. 1).

Despite these similarities between the BG/GCL and SST/pollen records, some points of divergence also exist which, while possibly attributable to site-specific environmental shifts or in-cave processes, also raise questions about non-stationarity in the connections between ocean conditions and Iberian climate (Fig. 7). For example, some marine cores reveal a prominent spike in forest taxa occurring at the start of interglacials, decreasing thereafter for the next 5-10 kyr (Tzedakis et al, 2004; Desprat et al., 2007). This early interglacial peak is a common feature in several time series including the Antarctic δD (Petit et al., 1999) and CH_4 records (Loulergue et al., 2008), and in stalagmite isotopic ratios from the eastern Mediterranean (Bar-Matthews et al., 2003) and southern France (Couchoud et al., 2009) (Fig. 2). However, the BG/GCL $\delta^{13}C$ record lacks this feature.

Next, stalagmite $\delta^{13}C$ values are lower during GI 20-22 (MIS 5a/4; 84-72 ka) than in either the Holocene or MIS 5e, suggesting that maximum warmth and precipitation were not coincident with peak summer insolation (~127 ka) (Fig. 6). BG/GCL $\delta^{234}U$ values support this interpretation and compare well with the carbon isotope ratios from the same samples, which are substantially lower during GI 20-22 than in the Holocene. This interval is of particular interest given that Atlantic forest pollen, which has been used as a proxy for air temperature, was decoupled from SST across northwestern Iberia during cold events (C18-C20) (Rousseau et al., 2006; Rasmussen et al., 2014). This decoupling is interpreted to reflect a weakened control of SST on Iberian atmospheric temperature that, in turn, drove enhanced transport of atmospheric vapor to the high latitudes, amplifying production of ice sheets in the early stages of the last glacial cycle (Sánchez Goñi et al., 2013); this process has also been demonstrated for an earlier interglacial (MIS 19; Sánchez Goñi et al., 2016). And while the BG/GCL $\delta^{13}C$ record generally tracks SST, an anomalously large $\delta^{13}C$ response marks ice rafting event C24 (111-108 ka), with $\delta^{13}C$ values rising ~5‰ higher than expected based on the observed scaling with SST (Fig. 7).

One possible explanation for these relationships is disequilibrium effects on speleothem isotopic ratios, although overlap of coeval stalagmites generally supports a consistent climatic mechanism. Alternatively, changes in the nature of the NAO may have occurred over millennial time scales, with persistent positive (negative) NAO modes having been proposed for GS (GI) (Moreno et al., 2002; Sánchez Goñi et al., 2002; Daniau et al., 2007) as well as centennial periods during the Holocene (Chabaud et al., 2014), which resulted in sustained changes in precipitation regime. The dynamics of the NAO and Azores High pressure system are not well understood prior to the historical era (Trouet et al., 2009), and the BG/GCL record cannot address this question independently. However, Justino and Peltier (2005) modeled the NAO during the LGM and found fundamental differences as compared to modern conditions, including pronounced southerly, rather than westerly, atmospheric flow during positive NAO phases.

One test of past NAO dynamics involves spatial variations in precipitation across Iberia. Rainfall variability in eastern Iberia is less closely tied to the NAO than is western Iberia and instead reflects other climatic phenomena including the El Niño-Southern Oscillation (Rodó et al., 1997), helping to produce an east-west precipitation gradient. Pollen spectra from the southwest Portuguese margin and those from the Alboran Sea in the western Mediterranean (Fig. 1) reveal a pronounced precipitation gradient during HS. This interpretation is supported by varying abundances of aeolian debris (including charcoal) deposited in marine deposits in the western Mediterranean that may reflect distinct wind patterns associated with NAO modes (Combourieu-Nebout et al., 2002), talthough contradictory results were obtained by Daniou et al. (2007). And Naughton et al. (2009) identified distinct climatic phases within HS consistent with changes in the NAO phasing. Additional speleothem records offering greater spatial coverage across Iberia will provide a more robust test of the underlying drivers of millennial-scale hydroclimatic changes during recent glacial periods.

6. Conclusions

Throughout most of the last two glacial cycles, hydroclimate and vegetation dynamics at BG and GCL closely tracked North Atlantic SST over both orbital and millennial scales. Enhanced aridity characterized HS, as evidenced by hiatuses in stalagmite growth or elevated carbon isotopic ratios. While not fully understood, evidence suggests that $\delta^{13}C$ variability at these scales was tied to enhanced prior calcite precipitation or depressed soil respiration rates. Differences between the structure of the stalagmite and SST records during some time intervals suggest that land-sea connections across Iberia may have varied temporally and spatially. In order to further test this hypothesis, additional speleothem records should be developed from central and southern Iberia to better constrain spatial patterns of glacial hydroclimate variability.

Acknowledgements

This work was supported by the Center for Global and Regional Environmental Research and Cornell College (to R.F.D.), and the U.S. National Science Foundation (grant BCS-1118155 to J.A.H., BCS-1118183 to M.M.B., and AGS-135539 to C.C.U.). Field sampling performed under the auspices of IGESPAR (to J.A.H.) and Associação de Estudos Subterrâneos e Defesa do Ambiente. Brandon Zinsious and Stephen Rasin contributed to fieldwork at BG, and Zachary LaPointe assisted with radioisotopic analyses; Suzanne Ankerstjerne performed stable isotope measurements. This manuscript benefitted from discussions with Maria F. Sánchez Goñi, David Hodell, and Chronis Tzedakis. Stable and U-series isotope data are available at the NOAA National Centers for Environmental Information website.

References

Asmerom, Y., Polyak, V., Burns, S.: Variable winter moisture in the southwestern United States linked to rapid glacial climate shifts, Nat Geosci, 3, 114-117, 2010.

Baker, A., Ito, E., Smart, P., McEwan, R.: Elevated and variable values of ^{13}C in speleothems in a British cave system, Chem Geol, 136, 263-270, 1997.

Barker, S., Knorr, G., Edwards, R.L., Parrenin, F., Putnam, A.E., Skinner, L.C., Wolff, E., Ziegler, M.: 800,000 years of abrupt climate variability, Science, 334, 347-351, 2011.

Bar-Matthews, M., Ayalon, A., Gilmour, M., Matthews, A., Hawkesworth, C.J.: Sea-land oxygen isotopic relationships from planktonic foraminifera and speleothems in the Eastern Mediterranean region and their implication for paleo-rainfall during interglacials intervals, Geochim Cosmochim Ac, 67, 3181–3199, 2003.

Barnston, A.G. and Livezey, R.E.: Classification, seasonality, and persistence of low-frequency atmospheric circulation patterns, Mon Weather Rev, 115, 1083–1126, 1987.

Blanco Castro, E., Casado González, M.A., Costa Tenorio, M., Escribano Bombín, R., García Antón, M., Génova Fuster, M., Gómez Manzaneque, F., Gómez Manzaneque, A., Moreno Sáiz, J.C., Morla Juaristi, C., Regato Pajares, P., Sáiz Ollero, H.: Los bosques ibéricos. Planeta, Barcelona, 1997.

Boch, R., Cheng, H., Spötl, C., Edwards, R.L., Wang, X., Hauselmann, Ph.: NALPS: a precisely dated European climate record 120-60 ka, Clim Past, 7, 1049-1072, 2011.

Breitenbach, S.F.M., Rehfeld, K., Goswami, B., Baldini, J.U.L., Ridley, H.E., Kennett, D.J., Prufer, K.M., Aquino, V.V., Asmerom, Y., Polyak, V.J., Cheng, H., Kurths, J., Marwan, N.: Constructing proxy records from age models (COPRA), Clim Past, 8, 1765-1779, 2012.

Clim. Past Discuss., https://doi.org/10.5194/cp-2017-146
Manuscript under review for journal Clim. Past
Discussion started: 24 November 2017

Breitenbach, S.F.M., Lechleitner, F.A., Meyer, H., Diengdo, G., Mattey, D., Marwan, N.: Cave ventilation and rainfall signals in dripwater in a monsoonal setting – a monitoring study from NE India, Chem Geol, 402, 111-124, 2015.

Chabaud, L., Sánchez Goñi, M.F., Desprat, S., Rossignol, L.: Land-sea climatic variability in the eastern North Atlantic subtropical region over the last 14,200 years: Atmospheric and oceanic processes at different timescales Holocene, 24, 787-797, 2014.

Chabaux, F., Riotte, J., Dequincey, O.: U–Th–Ra fractionations during weathering and river transport. Rev Mineral Geochem, 52, 533–576. 2003.

Collister, C. and Mattey, D.: Controls on water drop volume at speleothem drip sites: An experimental study. J Hydrol, 358, 259-267, 2008.

Combourieu-Nebout, N., Turon, J.L., Zahn, R., Capotondi, L., Londeix, L., Pahnke, K.: Enhanced aridity and atmospheric high-pressure stability over the western Mediterranean during the North Atlantic cold events of the past 50 k.y. Geology, 30, 863–866, 2002.

Combourieu-Nebout, N., Peyron, O., Dormoy, I., Desprat, S., Beaudouin, C., Kotthoff, U., Marret, F.: Rapid climatic variability in the west Mediterannean during the last 25 000 years from high resolution pollen data, Clim Past, 5, 503-521, 2009.

Cortesi, N., Gonzalez-Hidalgo, J.C., Trigo, R.M., and Ramos, A.M.: Weather types and spatial variability of precipitation in the Iberian Peninsula, International Journal of Climatology, 34, 2661-2677.

Couchoud, I, Genty, D., Hoffman, D., Drysdale, R., Blamart, D.: Millennial-scale climate variability during the Last Interglacial recorded in a speleothem from south-western France. Quaternary Sci Rev, 28, 3263-3274, 2009.

Daniou, A.-L., Sánchez Goñi, M.F., Beaufort, L., Laggoun-Defarge, F., Loutre, M.-F., Duprat, J.: Dansgaard-Oeschger climatic variability revealed by fire emissions in southwestern Iberia. Quaternary Sci Rev, 26, 1369-1383, 2007.

Darfeuil, S., Ménot, G., Giraud, X., Rostek, F., Tachikawa, K., Garcia, M., Bard, É.: Sea surface temperature reconstructions over the last 70 kyr off Portugal: Biomarker data and regional modeling, Paleocean, 31, 40–65, 2016.

de Abreu, L., Shackleton, N.J., Schönfeld, J., Hall, M., and Chapman, M.: Millennial-scale oceanic climate variability off the Western Iberian margin during the last two glacial periods, Marine Geol, 196, 1-20, 2003.

Denniston, R.F., González, L.A., Asmerom, Y., Baker, R.G., Reagan, M.K. Bettis, E.A. III.: Evidence for increased cool season moisture during the middle Holocene, Geology, 27, 815-818, 1999.

Desprat et al.: Climatic variability of Marine Isotope Stage 7: direct land-sea-ice correlation from a multiproxy analysis of a north-western Iberian margin deep-sea core. Quaternary Sci Rev 25, 1010-1026, 2006.

Desprat, S., Sánchez Goñi, M.F., Naughton, F., Turon, J.-L., Duprat, J., Malaizé, B., Cortijo, E., Peypouquet, J.-P.: Climate variability of the last five isotopic interglacials: Direct land-sea-ice correlation from the multiproxy analysis of North-Western Iberian margin deep-sea cores, Editor(s): F. Sirocko, M. Claussen, M.F. Sánchez Goñi, T. Litt *In* Developments in Quaternary Sciences, Elsevier, pp. 375-386, 2007.

Dorale, J. A., González, L. A., Reagan, M. K., Pickett, D. A., Murrell, M. T., and Baker, R. G.: A high-resolution record of Holocene climate change in speleothem calcite from Cold Water Cave, northeast Iowa, Science, 258, 1626-1630, 1992.

Dorale, J.A., and Liu, Z.: Limitations of Hendy Test criteria in judging the paleoclimatic suitability of speleothems and the need for replication. J Cave Karst Stud, 71, 73-80, 2009.

Eynaud et al.: Position of the Polar Front along the western Iberian margin during key cold episodes of the last 45 ka, Geochem Geophy Geosys, 10, Q07U05, doi:10.1029/2009GC002398, 2009.

d'Erico, F. and Sánchez Goñi, M.F.: Neanderthal extinction and the millennial scale climatic variability of OIS 3. Quaternary Sci Rev, 22, 769-788, 2003.

Fairchild, I.J., Smith, C.L., Baker, A., Fuller, L., Spötl, C., Mattey, D., McDermott, F., E.I.M.F.: Modification and preservation of environmental signals in speleothems. Earth Sci Rev 75, 105-153, 2006.

Fankhauser, A., McDermott, F., and Fleitmann, D.: Episodic speleothem deposition tracks the terrestrial impact of millennial-scale last glacial climate variability in SW Ireland, Quaternary Sci Rev, 152, 104-117, 2016.

Fletcher, W.J., Sánchez Goñi, M.F., Allen, J.R.M., Cheddadi, R., Combourieu-Nebout, N., Huntley, B., Lawson, I., Londiex, L., Magri, D., Margari, v., Müller, U.C., Naughton, F., Novenko, E., Roucoux, K., Tzedakis, P.C.: Millennial scale variability during the last glacial in vegetation records from Europe. Quaternary Sci Rev, 29, 2839-2864, 2010.

Genty, D., Blamart, D., Ouahdi, R., Gilmour, M., Baker, A., Jouzel, J., Van-Exter, S.: Precise dating of Dansgaard-Oeschger climate oscillations in western Europe from stalagmite data, Nature, 421, 833-837, 2003.

Gimeno, L., Stohl, A., Trigo, R.M., Dominguez, F., Yoshimura, K., Yu., L., Drumond,A., Durán-Quesada, A.M., Nieto, R.: Oceanic and terrestrial sources of continental precipitation. Rev Geophy, 50, 1-41, 2012.

Clim. Past Discuss., https://doi.org/10.5194/cp-2017-146
Manuscript under review for journal Clim. Past
Discussion started: 24 November 2017

Gómez-Orellana, L., Ramil-Rego, P., & Sobrino, C. M.: The Würm in NW Iberia, a pollen record from Area Longa (Galicia). Quaternary Res, 67, 438-452, 2008.

Hellstrom, J. and McCulloch, M.: Multi-proxy constraints on the climatic significance of trace element records from a New Zealand speleothem. Earth Planet Sc Lett, 179, 287-297, 2000.

Hodell, D., Crowhurst, S., Skinner, L., Tzedakis, P.C., Margari, V., Channell, J.E.T., Kamenov, G., Maclachlan, S., Rothwell, G.: Response of Iberian margin sediments to orbital and suborbital forcing over the past 420 ka, Paleoceanography, 28, 185-199, 2013.

Hodge, E.J., Richards, D.A., Smart, P.L., Andreo, B., Hoffman, D.L., Mattey, D.P., Gonzales-Ramon, A.: Effective precipitation in southern Spain (~266 to 46 ka) based on a speleothem stable carbon isotope record. Quaternary Res, 69, 447-457, 2008.

IAEA/WMO: Global Network of Isotopes in Precipitation. The GNIP Database. Accessible at: http://www.iaea.org/water, 2016.

Instituto de Meteorologia IP Portugal: Climate Normals: http://www.meteo.pt/en/oclima/clima.normais/015/ (accessed October 23, 2012).

Justino, F. and Peltier, W.R.: The glacial North Atlantic Oscillation. Geophysical Research Letters, 32, L21803, 2008.

Kim, S.-T. and O'Neil, J.R.: Equilibrium and nonequilibrium oxygen isotope effects in synthetic carbonates: Geochim Cosmochim Ac, 61, 3461-3475, 1997

Lorenzo, M.N., Iglesias, I., Taboada, J.J., Gomez-Gesteira, M.: Relationship between monthly rainfall in northwest Iberian Peninsula and North Atlantic sea surface temperature. Int J Climatology, 30, 980-990, 2010.

Loulergue, L., Schilt, A., Spahni, R., Masson-Delmotte, V., Blunier, T., Lemieux, B., Barnola, J.-M., Raynaud, D., Stocker, T.F., Chappellaz, J.: Orbital and millennial-scale features of atmospheric CH4 over the past 800,000 years, Nature, 453, 383-386, 2008.

Margari, V., Skinner, L.C., Hodell, D.A., Martrat, B., Toucanne, S., Grimalt, J.O., Gibbard, P.L., Lunkka, J.P., Tzedakis, P.C.: Land-ocean changes on orbital and millennial time scales and the penultimate glaciation, Geology, 42, 183-186, 2014.

Martin-Vide, J. and Lopez-Bustins, J-A.: The Western Mediterranean Oscillation and rainfall in the Iberian Peninsula. Int J Climatol, 26, 1455-1475, 2006.

Martrat, B., Grimalt, J.O., Shackleton, N.J., de Abreu, L., Hutterli, M.A., Stocker, T.F.: Four climate cycles of recurring deep and surface water destabilizations on the Iberian margin, Science, 317, 502-507, 2007.

McManus, J.F., Oppo, D.W., Cullen, J.L.: A 0.5-Million-Year Record of Millennial-Scale Climate Variability in the North Atlantic, Science, 283, 971-975, 1999.

Mickler, P.J. et al.: Stable isotope variations in modern tropical speleothems: Evaluation equilibrium vs. kinetic isotope effects. Geochim Cosmochim Acta. 68, 4381-4393, 2004.

Moreno, A., Cacho, I., Canals, M., Prins, M.A., Sánchez Goñi, M.F., Grimalt, J.O., Weltje, G.J: Saharan dust transport and high-latitude glacial climate variability: the Alboran Sea record. Quaternary Res, 58, 318-328, 2002.

Moreno, A., Gonzalez-Samperiz, P., Morellon, M., Valero-Garces, B.L., Fletcher, W.J.: Northern Iberian abrupt climate change dynamics during the last glacial cycle: a view from lacustrine sediments. Quaternary Sci Rev, 36, 139-153, 2012.

Moreno, A., Sancho, C., Bartolumé, M., Oliva-Rucia, B., Delgado-Huertas, A., José, Estrela, M., Corell, D., López-Moreno, J.I., Cacho, I.: Climate controls on rainfall isotopes and their effects on cave drip water and speleothem growth: the case of Molinos cave (Teruel, NE Spain). Clim Dyn, 43, 221-241, 2014.

Moseley, G.E., Spötl, C., Scensson, A., Cheng, H., Brandstatter, S., Edwards, R.L.: Multi-speleothem record reveals tightly coupled climate between central Europe and Greenland during Marine Isotope Stage 3. Geology, 42, 1043-1946, 2014.

Naughton, F., Sánchez Goñi, M.F., Desprat, S., Turon, J.-L., Duprat, J., Malaizé, B., Joli, C., Cortijo, E., Drago, T., Freitas, M.C.: Present-day and past (last 25,000 years) marine pollen signal off western Iberia. Mar Micropaleontol, 62, 91–114, 2007.

Naughton, F., Sánchez Goñi, M.F., Kageyama, M., Bard, E., Duprat, J., Cortijo, E., Desprat, S., Malaizé, B., Joly, C., Rostek, F., Turon, J.-L.: Wet to dry climatic trend in north-western Iberia within Heinrich events. Earth Planet Sc Lett, 284, 329-342, 2009.

North Greenland Ice Core Project members: High-resolution record of Northern Hemisphere climate extending into the last interglacial period, Nature, 431, 147-151, 2004.

Oster, J.L., Ibarra, D.L., Harris, C.H., Maher, K.: Influence of eolian deposition and rainfall amounts on the U-isotopic composition of soil water and soil minerals. Geochim Cosmochim Ac, 88, 146 – 166, 2012.

Paredes, D., Trigo, R.M., Garcia-Herrera, R., Franco Trigo, I.: Understanding precipitation changes in Iberia in early spring: weather typing and storm-tracking approaches. J Hydrometeorol, 7, 101-113, 2006.

Petit, J.R., Jouzel, J., Raynaud, D., Barkov, N.I., Barnola, J.-M., Basile, I., Bender, M., Chappellaz, J., Davis, M., Delaygue, G., Delmotte, M., Kotlyakov, V.M., Legrand, M., Lipenkov, V.Y., Lorius, C., Pepin, L., Ritz, C., Saltzman, E., Stievenard, M.: Climate and atmospheric history of the 420,000 years from the Vostok ice core, Antarctica. Nature, 399, 429-436, 1999.

Plagnes, V., Causse, C., Genty, D., Paterne, M., Blamart, D.: A discontinuous climatic record from 187 to 74 ka from a speleothem of the Clamouse Cave (south of France). Earth Planet Sci Lett, 201, 87-103, 2002.

Polyak, V.J., Asmerom, Y., Burns, S.J., and Lachniet, M.S.: Climatic backdrop to the terminal Pleistocene extinction of North American mammals, Geology, 40, 1023-1026, 2012.

Rasmussen, S.O. et al.: A stratigraphic framework for abrupt climatic changes during the Last Glacial period based on three synchronized Greenland ice-core records: redefining and extending the INTIMATE event stratigraphy, Quaternary Sci Rev, 106, 14–28, 2014.

Rey Benayas, J.M. and Scheiner, S.M.: Plant diversity, biogeography and environment in Iberia: Patterns and possible causal factors. J Veg Sci, 13, 245-258, 2002.

Ridley, H.E. et al.: Aerosol forcing of the position of the intertropical convergence zone since AD 1550, Nat Geosci, 8, 195-200, 2015.

Rodó, X., Baert, E., Comin, F.A.: Variations in seasonal rainfall in Southern Europe during the present century: relationships with the North Atlantic Oscillation and the El Niño-Southern Oscillation. Clim Dynam, 13, 275-284 1997.

Rodrigues et al.: The last glacial-interglacial transition (LGIT) in the western mid-latitudes of the North Atlantic: Abrupt sea surface temperature change and sea level implications. Quaternary Sci Rev, 29, 1853-1862, 2010.

Roucoux, K.H., de Abreu, L., Shackleton, N.J., Tzedakis, P.C.: The response of NW Iberian vegetation to North Atlantic climate oscillations during the last 65kyr, Quaternary Sci Rev, 24, 1637-1653, 2005.

Roucoux, K.H., Tzedakis, P.C., de Abreu, L., Shackleton, N.J.: Climate and vegetation changes 180,000 to 345,000 years ago recorded in a deep-sea core off Portugal. Earth Planet Sci Lett, 249, 307-325, 2006.

Rousseau, D.D., Kukla, G., McManus, J.: What is what in the ice and the ocean? Quaternary Sci Rev, 25, 2025-2030, 2006.

Sánchez Goñi, M.F., Turon, J.L., Eynaud, F., Gendreau, S., European climatic response to millennial-scale changes in the atmosphere-ocean system during the Last Glacial Period. Quaternary Res, 54, 394-403, 2000.

Sánchez Goñi, M.F., Cacho, I., Turon, J-L., Guiot, J., Sierro, F.J., Peypouquet, J.-P., Grimalt, J.O., Shackleton, N.J.: Synchroneity between marine and terrestrial responses to millennial scale climatic variability during the last glacial period in the Mediterranean region. Clim Dynam, 19, 95-105, 2002.

Sánchez Goñi, M.F., Landais, A., Fletcher, W.J., Naughton, F., Desprat, S., Duprat, J.: Contrasting impacts of Dansgaard-Oeschger events over a western European latitudinal transect modulated by orbital precession. Quaternary Sci Rev, 27, 1136-1151, 2008.

Sánchez Goñi, M.F., Bard, E., Landais, A., Rossignol, L., d'Errico, F.: Air-sea temperature decoupling in western Europe during the last interglacial-glacial transition. Nat Geosci, 6, 837-841, 2013.

Sánchez Goñi, M.F., Rodrigues, T., Hodell, D.A., Polanco-Martinez, J.M., Alonso-Garcia, M., Hernandez-Almeida, I., Desprat, S., Ferretti, P.: Tropically-driven climate shifts in southwestern Europe during MIS 19, a low eccentricity interglacial. Geophys Res Abst, 18, EGU2016-3940, 2016.

Schneider, U., Becker, A., Finger, P., Meyer-Christoffer, A., Ziese, M., Rudolf, B.: GPCC's new land surface precipitation climatology based on quality-controlled in situ data and its role in quantifying the global water cycle. Theoret Appl Climatol, 115, 15-40, 2013.

Spötl, C., Mangini, A., Richards, D.A.: Chronology and paleoenvironment of Marine Isotope Stage 3 from two high-elevation speleothems, Austrian Alps. Quaternary Sci Rev, 25, 1127-1136, 2006.

Stoll, H.M., Moreno, A., Mendez-Vincente, A., Gonzalez-Lemos, S., Jimenez-Sánchez, M., Dominguez-Cuesta, M.J., Edwards, R.L., Cheng, H., Wang, X.: Paleoclimate and growth rates of speleothems in the northwestern Iberian Peninsula over the last two glacial cycles. Quaternary Res, 80, 284-290, 2013.

Trigo, R.M., Osborn, T.J., Corte-Real, J.M.: The North Atlantic Oscillation influence on Europe: climate impacts and associated physical mechanisms, Clim Res, 20, 9-17, 2002.

Trouet, V., Esper, J., Graham, N.E., Baker, A., Scourse, J.D., Grank, D.C.: Persistent positive North Atlantic Oscillation mode dominated the Medieval Climate Anomaly. Science, 324, 78-80, 2009.

Tzedakis, P.C., Roucoux, K.H., de Abreu, L., Shackleton, N.J.: The duration of forest stages in southern Europe and interglacial climate variability, Science, 306, 2231-2235, 2004.

Vaks, A., Gutareva, O.S., Breitenbach, S.F.M., Avirmed, E., Mason, A.J., Thomas, A.L., Osinev, A.V., Kononov, A.M., Henderson, G.M.: Speleothems reveal 500,000-year history of Siberian permafrost. Science, 340, 183-186, 2013.

Vandenberghe, J., French, H.M., Gorbunov, A., Marchenko, S., Velichko, A.A., Jin, H., Cui, Z., Zhang, T.,Wan, X.: The Last Permafrost Maximum (LPM) map of the Northern

Hemisphere: permafrost extent and mean annual air temperatures, 25-17 ka BP, Boreas, 43, 652–666, 2014.

Vegas, J., Ruiz-Zapata, B., Ortiz, J.E., Galan, L., Torres, T., Garcia-Cortes, A., Gil-Garcia, M.J., Perez-Gonzalez, A., Gallardo-Millan, J.L.: Identification of arid phases during the last 50 cal. ka BP from the Fuentillejo maar-lacustrine record (Campo de Calatrava Volcanic Field, Spain), J Quaternary Sci, 25, 1051-1062, 2010.

Voelker, A.H. L., Rodrigues, T., Stein, R., Hefter, J., Billups, K., Oppo, D., McManus, J,, Grimalt, J.O.: Variations in mid-latitude North Atlantic surface water properties during the mid-Brunhes (MIS 9-14) and their implications for thermohaline circulation, Clim Past, 6, p. 531-552, 2010.

Voelker, A.H.L. and de Abreu, L.: A review of abrupt climate change events in the northeastern Atlantic Ocean (Iberian Margin): Latitudinal, Longitudinal, and Vertical Gradients. Abrupt Climate Change: Mechanisms, Patterns, and Impacts (Eds. Rashid, H., Polyak, L., and Mosley-Thompson, E.), Geophysical Monograph Series 193, 15-37, 2011.

Figure Captions

Figure 1. Average annual precipitation (mm) of the Iberian Peninsula for years AD 1901-2009 (GPCC v. 6; Schneider et al., 2013) relative to cave study sites (white stars: GLC = Gruta do Casal de Libre; BG = Buraca Gloriosa). Rectangle denotes location of northwest Spain cave sites (NWSC) (Moreno et al., 2010; Stoll et al., 2013); FM = Fuentillejo maar (Vegas et al., 2010) and GT = Gitana cave (Hodge et al., 2008); VC = Villars Cave (Genty et al., 2003) located just north of map. Also shown are locations of marine cores discussed in text and GNIP

Clim. Past Discuss., https://doi.org/10.5194/cp-2017-146
Manuscript under review for journal Clim. Past
Discussion started: 24 November 2017

station at Porto. Bathymetric contours shown in grey (m). Location of currents after Voelker et al. (2010).

Figure 2. Environmental monitoring at BG. A. Comparison of rainfall data from Monte Real weather station (proximal to BG) and drip rates at BG. B. Temperature and humidity at BG. C. Temperature and humidity profiles at GCL.

Figure 3. Oxygen isotopic composition of precipitation and rainfall amount (lefthand panels) and air temperature (righthand panels). Data collected at IAEA/GNIP site in Porto, Portugal (see Fig. 1 for location). Oxygen isotope data represent multi-year averages of monthly means. Note that righthand y-axis in upper left panel is inverted in order to illustrate inverse nature of rainfall and precipitation oxygen isotopic composition.

Figure 4. Iberian rainfall anomalies associated with the NAO. Precipitation anomalies, averaged for November-March, between the positive NAO winter of 1988/89 (top panel) or the negative NAO winter of 2009/2010 (bottom panel) relative to 1901-2013. Data from GPCC (v7) (Schneider et al, 2013). Yellow stars denote cave sites in this study: BG = Buraca Gloriosa; GCL = Gruta do Casal de Lebre. FM = Fuentillejo maar (Vegas et al., 2010) and GT = Gitana cave (Hodge et al., 2008).

Figure 5. COPRA-derived age models for BG/GCL stalagmites. Black lines represent mean of calculated age models while red lines denote 95% confidence intervals. See Table 1 for specific ages and isotopic ratios. Not shown is the age model for BG68, which is based on only two dates and thus was determined using linear interpolation. Orange squares represent “dummy

ages" that were included in order to be able to extrapolate below some hiatuses, which is only possible with at least two dated points. These dummy ages are added using the simple assumptions of i) stratigraphically correct growth slope (i.e. higher = younger) and ii) samples physically below a hiatus must be older than the oldest age above that hiatus. Conservative errors were added to account for the unknown "true" age of the stalagmite at these points.

Figure 6. Comparison of Portuguese stalagmite hydroclimate proxies with regional and global climate records from the last two glacial cycles (a) Ice-rafted debris abundance from North Atlantic ODP Site 980 (McManus et al., 1999 using Hulu cave time scale as presented in Barker et al., 2011); (b) BG/GCL stalagmite carbon isotopic time series with each stalagmite represented by a different color; ^{230}Th ages and 2 s.d. errors shown as circles with horizontal lines. Uranium isotopic ratios for stalagmite BG6LR denoted by blue diamonds. Increased δ^{13}C and δ^{234}U values indicate enhanced aridity; (c) Alkenone-based Iberian margin SST reconstruction (core MD01-2443; Martrat et al., 2007 adapted to synthetic Greenland chronology of Barker et al., 2011 by Hodell et al., 2013). Also shown are intervals between periods of speleothem growth at caves in northern Spain (Stoll et al., 2013) and Villars Cave (Genty et al., 2003). See Fig. 1 for locations; (d) Temperate forest pollen abundance from marine cores listed in figure (Tzedakis et al., 2004; Sánchez Goñi et al., 2008; Sánchez Goñi et al., 2013; Margari et al., 2014); (e) Synthetic Greenland oxygen isotopic record (Barker et al., 2011); (f) EPICA Dome C atmospheric methane record (Loulergue et al., 2008) and marine isotope stages.

Figure 7. Covariations of Iberian hydroclimate, Iberian margin SST, and Iberian pollen. Top Panel: Composite BG/GCL stalagmite δ^{13}C time series and Iberian margin $U_{37}^{k\,\prime}$ SST

reconstruction for core MD01-2443 (Martrat et al., 2007; see Fig. 1). For ease of comparison to SST, GCL6 is shifted by 2‰ (original values in grey). Light blue vertical bands denote Heinrich and Cold events (data from McManus et al., 1999 using Hulu cave time scale as presented in Barker et al., 2011), some of which are labeled. Note correlation between hiatuses in stalagmite growth and periods of depressed SST. Bottom Panel: Composite BG/GCL stalagmite $\delta^{13}C$ time series (as in top panel) and Iberian margin temperate pollen (Tzedakis et al., 2004; Sánchez Goñi et al., 2008; Sánchez Goñi et al., 2013; Margari et al., 2014).

Figure 8. Comparison of select millennial events in the BG and Greenland ice records. Left: Portion of the last deglaciation showing the BG stalagmite response (green) to cold events: $\delta^{13}C$ increase during the YD and a hiatus during HS1. Also shown is the NGRIP oxygen isotopic time series (North Greenland Ice Core Project members, 2004) (blue); Right: GI/GS events 90-70 ka. Stratigraphic nomenclature from Rasmussen et al. (2014).

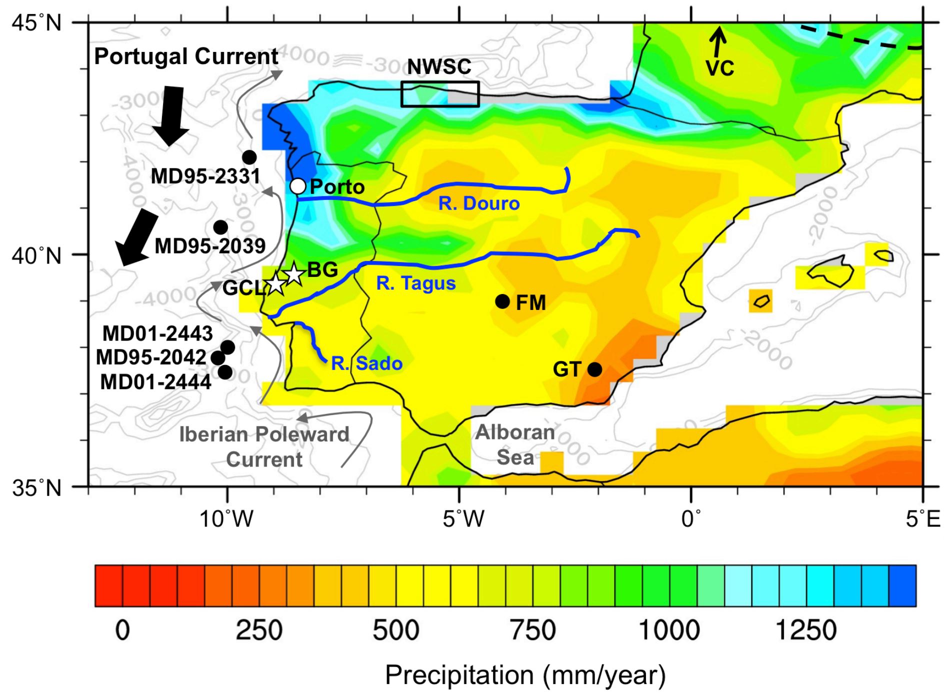

Figure 1.

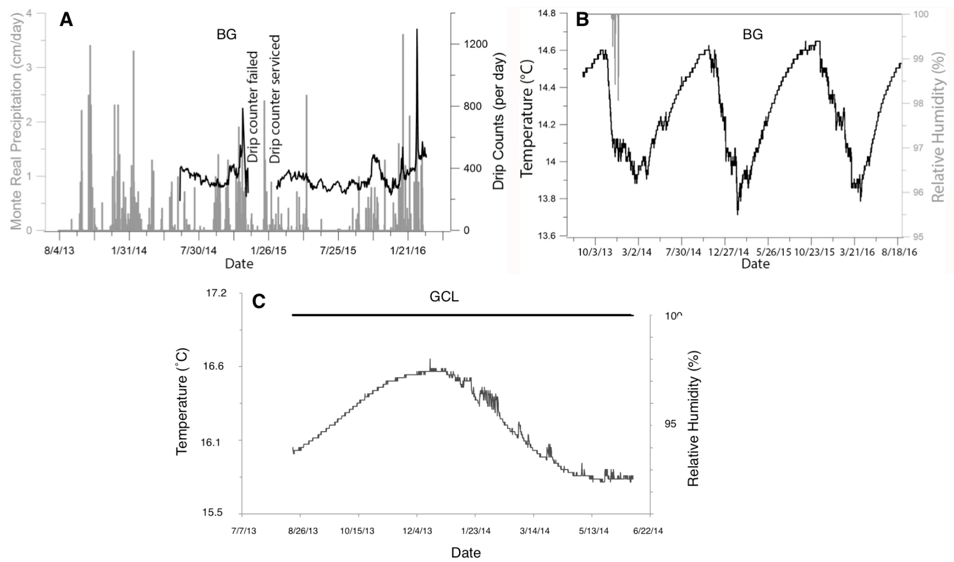

Figure 2.

Climate of the Past
Discussions
Open Access
EGU

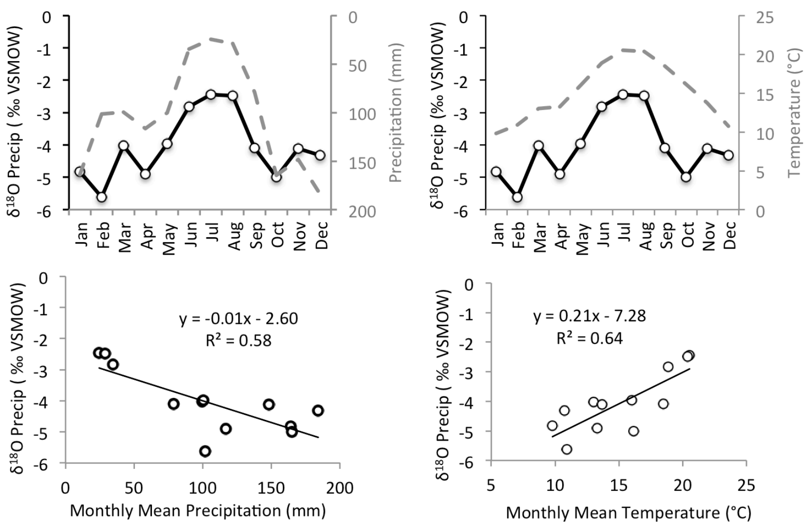

Figure 3.

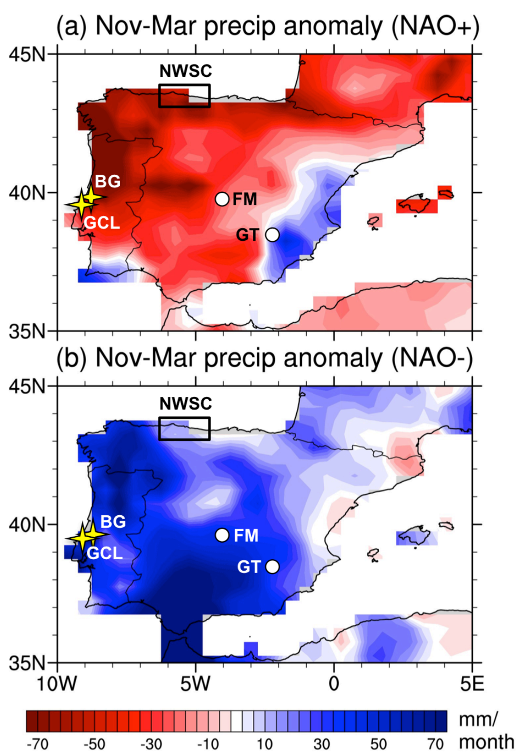

Figure 4.

Clim. Past Discuss., https://doi.org/10.5194/cp-2017-146
Manuscript under review for journal Clim. Past
Discussion started: 24 November 2017

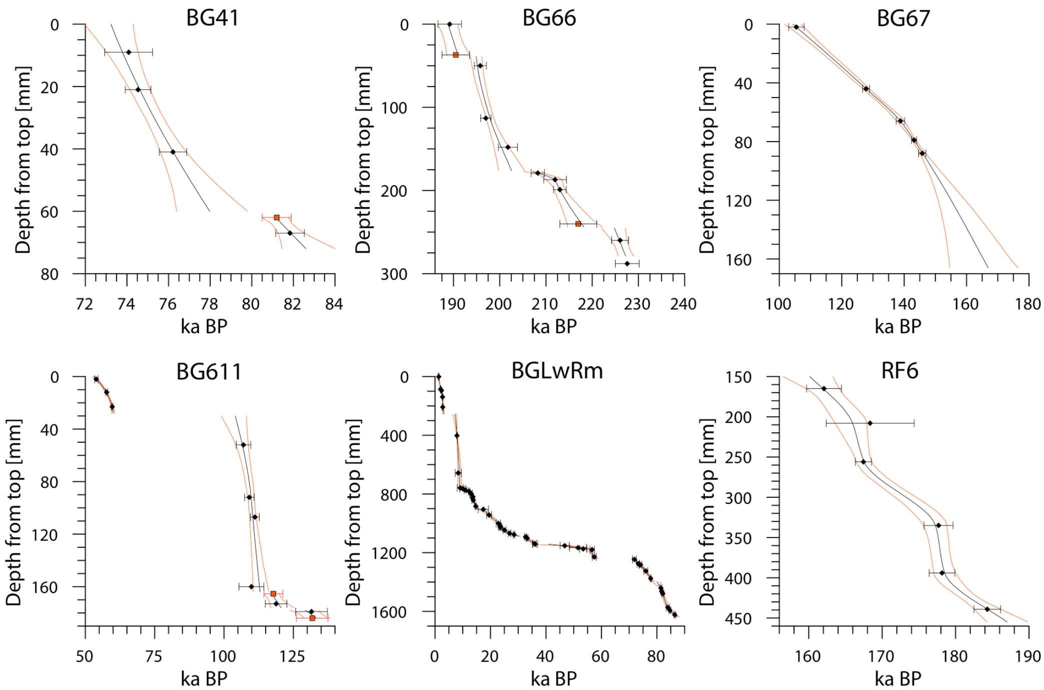

Figure 5.

Clim. Past Discuss., https://doi.org/10.5194/cp-2017-146
Manuscript under review for journal Clim. Past
Discussion started: 24 November 2017

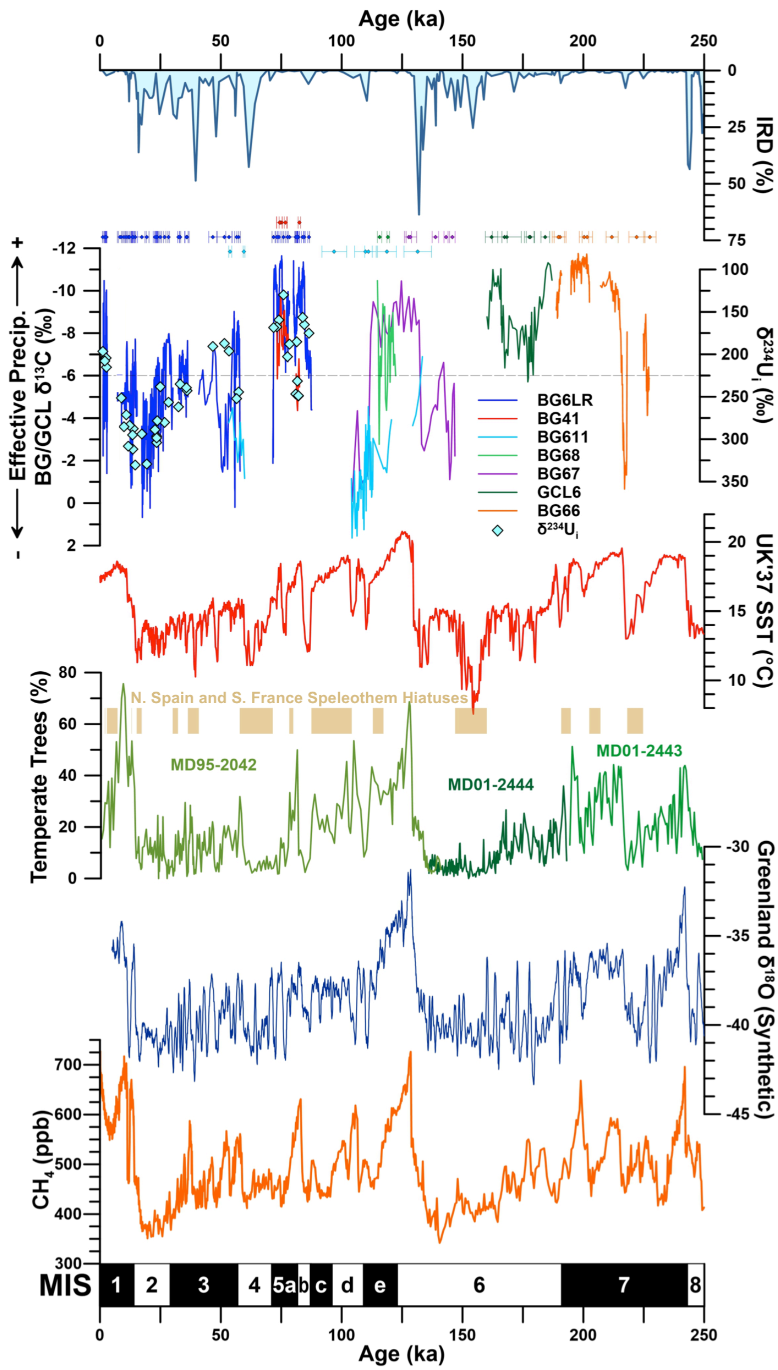

Figure 6.

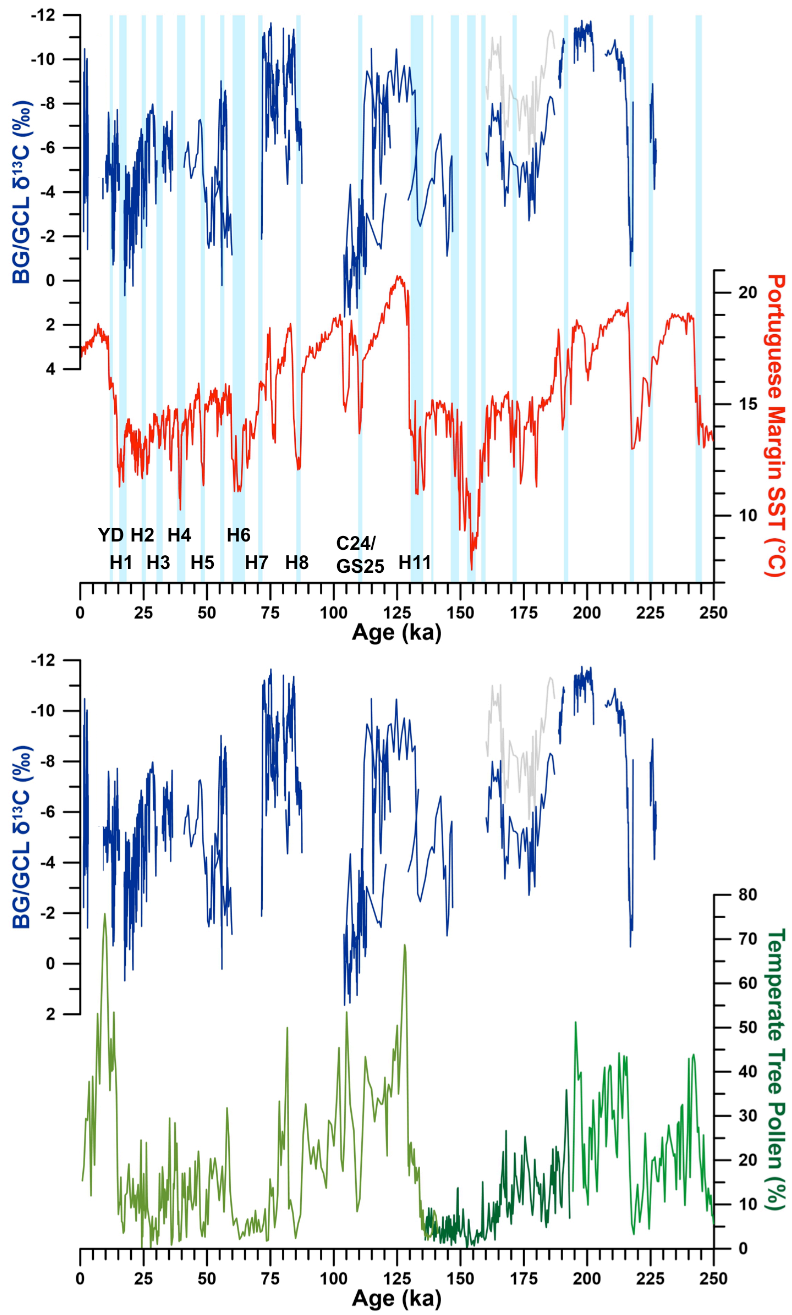
BG/GCL δ13C (‰)
Portuguese Margin SST (°C)
YD H1 H2 H3 H4 H5 H6 H7 H8
C24/
GS25
H11
Age (ka)
BG/GCL δ13C (‰)
Temperate Tree Pollen (%)
Age (ka)

Figure 7.

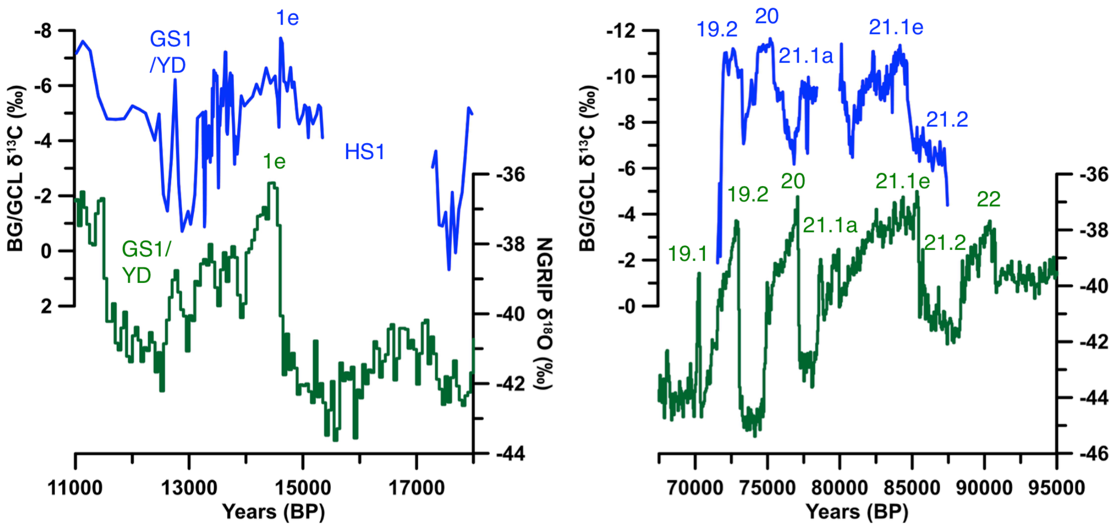
BG/GCL δ13C (‰)
GS1 /YD
1e
HS1
GS1/ YD
NGRIP δ18O (‰)
11000
13000
15000
17000
Years (BP)
19.2
20
21.1a
21.1e
21.2
19.1
22
70000
75000
80000
85000
90000
95000

Figure 8.

804

Clim. Past Discuss., https://doi.org/10.5194/cp-2017-146
Manuscript under review for journal Clim. Past
Discussion started: 24 November 2017

Climate of the Past
Discussions
Open Access

Table 1. Isotopic Ratios and ^{230}Th Ages

Stalagmite	Distance (mm)[a]	^{238}U (ng/g)	^{232}Th (pg/g)	δ^{234}U[b] (corr'd)	Error[c]	^{230}Th/^{238}U (activity)	Error	^{230}Th/^{232}Th (ppm)	Error	Uncorrected Age (yr BP)[d]	Error (yr)	Corrected Age (yr BP)[e]	Error (yr)
BG41	67	148	2,892	524.7	2.2	0.779	0.0023	657.7	18.6	82,926	389	82,553	538
BG41	41	293	4,635	522.8	2.2	0.742	0.0030	773.8	8.5	77,026	463	76,724	486
BG41	21	217	1,858	566.6	3.1	0.748	0.0039	1,440.0	40.6	74,906	567	74,746	588
BG41	9	271	2,088	610.8	9.8	0.764	0.0073	1,635.6	22.3	74,392	1,135	74,253	1,142
BG66	288	127	7,307	509.7	5.2	1.177	0.0025	338.3	2.5	231,038	1,960	227,590	2,562
BG66[f]	280	85	6,980	698.6	9.3	1.283	0.0057	256.5	1.8	223,637	3,252	219,220	3,829
BG66	260	84	3,481	709.4	4.5	1.291	0.0025	514.1	4.2	228,224	1,503	226,040	1,836
BG66	199	101	3,132	532.4	3.1	1.174	0.0015	623.6	4.6	214,835	1,052	213,011	1,379
BG66	187	75	4,657	429.2	3.8	1.116	0.0025	298.1	1.7	215,891	1,580	211,971	2,478
BG66	179	68	2,003	499.5	3.1	1.149	0.0019	644.2	7.4	210,002	1,175	208,236	1,456
BG66	148	95	4,336	379.4	3.1	1.073	0.0025	386.6	3.6	204,768	1,460	201,770	2,063
BG66	113	104	2,193	443.5	2.6	1.100	0.0015	864.2	11.9	198,297	930	196,990	1,128
BG66[f]	68	82	1,476	293.1	3.9	1.015	0.0030	933.1	29.6	200,740	1,920	199,494	2,275
BG66	50	104	2,661	345.4	2.4	1.041	0.0016	672.5	8.4	197,507	994	195,798	1,298
BG66[f]	24	91	6,080	389.7	5.1	1.061	0.0047	263.1	1.9	191,832	2,368	187,477	3,144
BG66	1	76	995	564.2	6.2	1.159	0.0057	1,453.3	64.3	189,936	2,538	189,182	2,549
BG67	88	320	2,153	617.8	2.9	1.095	0.0043	2,689.7	51.5	146,174	1,146	145,802	1,158
BG67	79	195	2,799	485.8	2.3	1.014	0.0022	1,164.3	18.2	144,037	695	143,171	814
BG67	66	250	4,187	610.3	4.9	1.072	0.0046	1,057.4	12.7	139,735	1,279	138,803	1,350
BG67	44	162	4,858	484.7	2.4	0.969	0.0023	531.9	5.3	129,620	608	127,800	1,087
BG67	2	216	5,542	401.5	2.6	0.837	0.0039	538.0	5.1	107,150	843	105,501	1,168
BG68	200	200	1,104	239.9	1.7	0.797	0.0017	2,382.0	66.9	119,376	509	119,247	525
BG68	80	199	317	273.0	2.2	0.802	0.0034	8,277.3	1,090.9	115,745	894	115,709	894
BG611	179	164	24,228	235.9	6.6	0.869	0.0046	97.1	0.5	142,696	1,841	131,493	5,716
BG611	173	119	11,744	202.6	3.5	0.801	0.0041	133.9	0.8	126,291	1,253	118,714	3,908
BG611	160	110	12,829	230.9	4.6	0.792	0.0044	112.1	0.7	118,612	1,277	109,828	4,469
BG611	107	99	3,304	238.0	3.0	0.776	0.0038	383.6	5.6	113,518	1,028	111,086	1,574
BG611	30	122	16,801	251.3	5.0	0.762	0.0043	91.2	0.5	107,202	1,088	96,920	5,126
BG611	23	313	552	340.8	1.4	0.553	0.0024	5,168.2	353.7	59,726	345	59,608	350
BG611	2	250	4,109	376.7	1.8	0.533	0.0021	535.0	5.9	54,959	284	53,887	604
BG6LR	1,623	72	133	175.0	1.5	0.631	0.0015	5,665.9	1,162.4	86,532	342	86,392	350
BG6LR	1,593	98	140	165.3	1.4	0.618	0.0014	7,166.0	1,764.0	84,748	318	84,639	324
BG6LR	1,574	74	905	156.6	1.6	0.615	0.0016	824.8	25.3	84,848	360	83,894	596
BG6LR	1478	159	26	249.2	1.8	0.645	0.0021	63,745.2	114,069.8	82,068	428	82,056	428
BG6LR	1464	166	1,138	246.8	1.5	0.641	0.0009	1,542.3	35.8	81,475	214	80,983	325
BG6LR	1442	162	77	185.4	1.4	0.634	0.6339	21,885.5	13,014.6	81,442	396	81,407	396
BG6LR	1375	112	220	202.9	1.5	0.602	0.6016	5,064.2	652.0	77,823	234	77,677	246
BG6LR	1324	120	1,908	130.2	1.4	0.566	0.5660	585.8	15.3	77,213	330	75,946	712
BG6LR	1283	132	1,019	159.5	2.0	0.566	0.5659	1,213.9	71.1	74,623	422	74,029	515
BG6LR	1276	105	353	167.8	2.1	0.564	0.5637	2,766.4	298.1	73,512	425	73,254	444
BG6LR	1246	83	1,232	168.7	1.4	0.561	0.5613	625.8	14.2	72,957	369	71,819	675
BG6LR	1179	62	1,114	252.0	2.6	0.507	0.5071	464.4	15.9	57,877	465	56,584	792
BG6LR	1174	77	2,544	196.0	2.2	0.474	0.4736	235.4	3.8	55,882	375	53,375	1,299
BG6LR	1166	5	367	187.1	2.6	0.482	0.4821	100.4	1.6	57,644	524	51,517	3,066
BG6LR	1153	81	3,460	190.7	2.2	0.433	0.4331	167.2	2.3	49,960	367	46,707	1,654
BG6LR	1141	52	1,159	242.6	2.8	0.359	0.3591	266.4	10.4	37,626	449	36,016	918
BG6LR	1138	55	750	239.5	1.8	0.352	0.3518	426.3	33.1	36,815	381	35,830	625
BG6LR	1101	71	283	235.2	2.0	0.323	0.3234	1,344.2	198.7	33,449	272	33,161	310
BG6LR	1093	70	472	262.1	2.1	0.327	0.3269	802.0	73.4	33,052	331	32,575	409
BG6LR	1077	101	595	256.6	1.8	0.290	0.2899	810.6	63.4	28,851	193	28,431	287
BG6LR	1068	85	1,034	280.0	1.4	0.285	0.2847	384.9	15.5	27,675	178	26,820	463
BG6LR	1046	56	705	238.2	2.2	0.260	0.2603	339.0	19.7	25,911	265	24,993	531
BG6LR	1026	123	2,093	304.1	1.9	0.262	0.2617	253.3	8.5	24,612	206	23,438	621
BG6LR	1025	123	493	296.4	1.4	0.253	0.0017	1,041.2	151.0	23,814	175	23,538	226
BG6LR	1019	80	377	298.5	2.1	0.252	0.2525	887.3	107.4	23,753	221	23,430	276
BG6LR	1001	68	1,464	288.7	1.5	0.256	0.2558	196.1	4.3	24,291	156	22,789	765
BG6LR	944	76	1,896	329.3	2.1	0.233	0.2330	154.8	3.9	21,131	196	19,450	861
BG6LR	899	79	4,209	294.0	3.4	0.227	0.2266	70.6	1.3	21,074	283	17,360	1,863
BG6LR	883	91	233	330.3	2.0	0.168	0.1684	1,082.0	213.7	14,806	165	14,633	189
BG6LR	843	100	1,409	287.7	4.0	0.162	0.1623	190.4	6.7	14,718	164	13,738	516
BG6LR	827	103	332	295.0	2.9	0.152	0.1521	783.5	116.9	13,645	154	13,424	192
BG6LR	819	75	491	311.6	1.4	0.158	0.1581	400.0	22.8	14,032	123	13,587	255
BG6LR	783	95	525	283.8	2.2	0.141	0.1406	418.7	35.3	12,661	150	12,275	246
BG6LR	774	107	1,351	271.4	1.4	0.130	0.1304	169.8	5.7	11,795	119	10,901	463
BG6LR	764	93	2,725	285.4	1.6	0.133	0.1334	75.3	1.6	11,942	141	9,892	1,031
BG6LR	759	135	4,177	251.5	1.5	0.121	0.1210	64.7	1.0	11,071	117	8,846	1,113
BG6LR	657	86	2,566	212.9	1.4	0.112	0.1120	62.1	0.9	10,540	96	8,326	1,106
BG6LR	139	172	323	204.2	1.7	0.031	0.0010	272.6	41.0	2,790	96	2,651	121
BG6LR	86	155	80	207.9	1.7	0.022	0.0007	720.9	312.3	1,987	62	1,949	67
BG6LR	1	122	43	196.7	18.9	0.014	0.0019	677.5	519.3	1,271	173	1,245	174
GCL6	439	91	2,815	76.3	2.3	0.862	0.0029	461.2	9.3	185,093	1,779	184,255	1,815
GCL6	394	86	3,009	125.7	2.0	0.881	0.0032	415.9	6.9	179,002	1,692	178,095	1,739

GCL6	335	70	4,579	82.7	3.0	0.856	0.0029	214.9	2.3	179,406	1,794	177,624	1,977
GCL6	256	116	1,019	86.2	2.2	0.836	0.0020	1,574.3	71.8	167,617	1,102	167,382	1,105
GCL6[f]	208	7	186	92.9	2.6	0.843	0.0124	522.0	99.0	169,018	6,007	168,307	5,988
GCL6	165	94	2,507	122.4	4.2	0.847	0.0049	526.3	13.4	162,712	2,368	162,022	2,550

[a] Distances are relative to the top of each stalagmite.
[b] $\delta^{234}U_{meas'd} = [(^{234}U/^{238}U)_{meas'd}/(^{234}U/^{238}U)_{eq}-1] \times 10^3$, where $(^{234}U/^{238}U)_{eq}$ is secular equilibrium activity ratio: $\lambda_{238}/\lambda_{234} = 1.0$. Values are reported as permil.
[c] Errors are 2σ.
[d] Present is defined as the year AD 1950.
[e] Initial $^{230}Th/^{232}Th$ atomic ratio of $13.5 \times 10^{-6} \pm 6.75 \times 10^{-6}$ used to correct for unsupported ^{230}Th.
[f] Not used in age model.